Nonlinear Dynamic RF System Characterization: Envelope Intermodulation Distortion Profiles--A Noise Power Ratio-Based Approach

Terms of use:

(Article begins on next page)

19 April 2024

Nonlinear Dynamic RF System Characterization: Envelope Intermodulation Distortion Profiles, a Noise Power Ratio Based Approach

Ricardo Figueiredo , *Graduate Student Member, IEEE*, Nuno Carvalho, *Fellow, IEEE*, Anna Piacibello, *Member, IEEE*, and Vittorio Camarchia, *Senior Member, IEEE*

Abstract—As radio-frequency (RF) applications occupy larger bandwidths, nonlinear dynamics become non-negligible. This work presents a theoretical framework capable of quantifying the impacts of nonlinear dynamic effects on RF systems through the observation of intermodulation distortion (IMD) profiles produced under multi-tone excitation. This framework defines static reference profiles, and quantifies inband nonlinear dynamic effects as the error between measured and reference profiles. This analysis demonstrates that classic linearity metrics, such as noise power ratio (NPR), adjacent channel power ratio, and co-channel power ratio do not have sufficient frequency resolution to reliably evaluate the impacts of nonlinear dynamics manifested in the IMD profiles produced by broadband RF systems. These observations result in a list of general characterization guidelines to overcome the limitations of classical linearity metrics in the assessment of nonlinear dynamics, and in the proposal and experimental validation of a novel method, swept-tone NPR, for the characterization of IMD profiles affected by nonlinear dynamic effects. Beyond this, the classic nonlinear dynamic mechanism, responsible for IMD asymmetry, is analyzed under multi-tone excitation at the system-level for the first time, and the limitations of mechanism based IMD analysis in the presence of nonlinear dynamic effects are evidenced with theoretical examples.

Index Terms—Characterization, intermodulation distortion, memory effects, multitone excitation, noise power ratio.

I. Introduction

MODERN radio-frequency (RF) communication systems, namely mobile and satellite applications, are occupying ever broader bandwidths and moving to higher frequency bands. This trend raises novel intermodulation distortion (IMD) characterization challenges, because nonlinear dynamic effects can no longer be neglected, thus the definition of appropriate IMD characterization techniques, and appropriate linearity metrics, becomes an increasingly complex problem. In the context of satellite applications, noise power ratio (NPR) has already been defined as the linearity criterion [1], [2], [3]. Beyond this, the establishment of an identity between NPR and error vector magnitude (EVM) [4], [5], [6], [7] makes NPR a consistent linearity metric in several levels of analysis, which is an indicator of its potential relevance for mobile applications as they move towards broader bandwidths. However, despite of the NPR inherent potential and initial hopes of its application in domains such as design optimization, behavioral modeling, memory effect characterization, and predistortion [2], [8], [9], it continues to be mostly used as a final design validation metric [10], [11], whereas simpler linearity metrics continue to be preferred for the aforementioned tasks.

Recently, it was demonstrated that unequally spaced multi-tone load-pull characterization techniques can be effectively used to guide power amplifier design trade-offs [12], [13]. This technique is compatible with classical NPR characterization in narrowband memoryless scenarios [14].

This was an important step towards the adoption of appropriate characterization techniques and appropriate linearity metrics in modern RF system design, as well as the development of novel instrumentation techniques that enable coherent vector signal analysis and facilitate the fast evaluation of NPR in modern equipment [15]. However, in the authors' opinion there are three major factors preventing the generalized use of NPR: 1) studies addressing NPR characterization often assume static nonlinearities [7], [16], considering only linear dynamic effects; 2) there is a lack of insight of how nonlinear dynamic effects can manifest in the IMD response under broadband excitation; 3) nonlinear dynamic effects imply a frequency dependent IMD response, but the cumulative nature of classic linearity metrics [17], such as NPR, adjacent channel power ratio (ACPR), and co-channel power ratio (CCPR) hide the frequency dependence of the IMD response. There is therefore a need to better understand how nonlinear dynamic effects manifest under broadband excitation, and to understand how to define linearity metrics to capture them.

The work presented in [18] was an important step towards the understanding of nonlinear dynamics in RF systems, as it

Ricardo Figueiredo, and Nuno Carvalho are with the Departamento de Eletrónica, Telecomunicações e Informática, Instituto de Telecomunicações, Universidade de Aveiro, Campus Universitário de Santiago, 3810-193 Aveiro, Portugal (e-mail: ricardofigueiredo@ua.pt; nbcarvalho@ua.pt).

Anna Piacibello is with the is with the Department of Electronics and Telecommunications, Politecnico di Torino, 10129 Turin, Italy, and also with the Microwave Engineering Center for Space Applications (MECSA), 00133 Rome, Italy (e-mail: anna.piacibello@polito.it).

Vittorio Camarchia is with the Department of Electronics and Telecommunications, Politecnico di Torino, 10129 Turin, Italy (e-mail: vittorio.camarchia@polito.it).

explains how memory effects can manifest through adjacent channel asymmetry observations. However, this explanation is presented in a circuit-level perspective that is hard to carry over to the system-level. Beyond this, the focus of the analysis is mostly on 2-tone characterization, while not expanding on the multi-tone scenario in a comprehensive manner. The work is also too tightly bound to specific third-order nonlinear dynamic mechanisms.

In [19], the multi-tone scenario is addressed, establishing a relationship between 2-tone and multi-tone measurements. This allowed the developments presented in [18] to be applied to compute multi-tone responses of nonlinear dynamic RF systems. The work presents a qualitative analysis of nonlinear dynamic effects, stating that these effects can be noted in the shape of distortion components, but a quantitative analysis is missing. The evaluation of IMD is done using ACPR and CCPR, which hide the frequency dependence of the IMD response. Beyond this, the nonlinear dynamic effect explanation remains at the circuit-level, despite the study being developed at the system-level, and the work remains too tightly bound to specific third-order nonlinear dynamic mechanisms. Furthermore, the use of 2-tone characterization is ultimately more laborious than multi-tone characterization, and has critical limitations regarding signal statistics, frequency domain resolution, and sensitivity.

These limitations of 2-tone characterization strategies have already been addressed in [20]. In that study an offset multi-sine strategy is proposed to characterize nonlinear dynamic RF systems. Offset multi-sines have the advantage of allowing for separate characterization of co-channel IMD distortion, and separate characterization of each nonlinear order, but the disadvantage of scalability as bandwidth, number of tones, and nonlinear order increase. In [20], a qualitative detection of nonlinear dynamic effects is observed through IMD spectral response variation as decoupling capacitors are adjusted, but an insightful analysis is missing.

In a previous work [21], we have already exposed the limitations of classic NPR characterization techniques to capture nonlinear dynamic effects within the system co-channel, and proposed a novel characterization procedure to overcome those limitations. However, despite insightful, this work lacks a formal representation of the IMD mechanisms, and a quantitative analysis of the proposed linearity metric.

In this work we:

1) Present a theoretical framework capable of analyzing IMD profiles produced under multi-tone excitation and detecting the impacts of nonlinear dynamic effects in a quantitative manner;
2) Analyze the classic nonlinear dynamic mechanism responsible for IMD asymmetry, presented in [18], under multi-tone excitation at the system-level for the first time;
3) Further expose the limitations of classic characterization techniques, and linearity metrics, to evaluate the IMD profiles affected by nonlinear dynamics;
4) Explain the limitations of mechanism based IMD analysis in the presence of nonlinear dynamic effects;

5) Detail general characterization guidelines for a reliable evaluation of dynamic IMD profiles, produced by nonlinear dynamic RF systems;
6) Propose a novel characterization method, swept-tone NPR, for the characterization of IMD profiles affected by nonlinear dynamic effects, and validate it experimentally.

This work is organized as follows. Section II presents the theoretical framework. Section III uses this framework to analyze the classic nonlinear dynamic mechanism at the system-level. Section IV analyzes three numerical dynamic IMD profile examples produced by the classic mechanism. The analysis focuses on the importance of defining reference responses, and on the limitations of classical linearity metrics. Section V addresses the limitations of mechanism based IMD analysis in the presence of nonlinear dynamic effects. Section VI discusses the implications of this work on characterization techniques and linearity metrics, detailing general characterization guidelines, and proposing a specific characterization method, swept-tone NPR. Section VII present the experimental validation of the swept-tone NPR characterization, which also serves as the experimental proof for the theoretical framework presented. Finally, Section VIII draws the major conclusions.

II. Nonlinear Dynamic RF Systems Revisited

This section presents the theoretical framework used throughout this work to analyze nonlinear dynamic effects in RF systems. Here, foundational concepts are revisited from the IMD profile point of view. This framework consists of a frequency domain analysis performed at the system-level, i.e. an analysis focused only on input/output signal observations. This contrasts with the conventional analysis performed at the circuit-level, focused on baseband impedance variation [18]. As stated, the object of the presented analysis is the spectral IMD profile produced under multi-tone excitation.

The aim is to use IMD profiles to measure nonlinear dynamic effects. This implies computing the static IMD profile, explaining how dynamic effects change the static IMD profile, and explaining how to measure those changes. The ultimate goal of this analysis is to provide insight on how to improve multi-tone linearity metrics, such as NPR, ACPR and CCPR, to be able to gauge nonlinear dynamic effects.

A. Static IMD Profile - Concept

Static nonlinear systems can be generally described by the polynomial in (1).

$$y_{\text{NL}}(t) = \sum_{n=0}^{\infty} a_n x(t)^n \qquad (1)$$

By shifting the analysis to the frequency domain it is easier to notice that, for a given excitation, each polynomial term imposes a specific spectral response profile. The linear spectral profile is an amplified replica of the input excitation spectrum, whereas each nonlinear profile can be obtained through the convolution theorem, as expressed in (2).
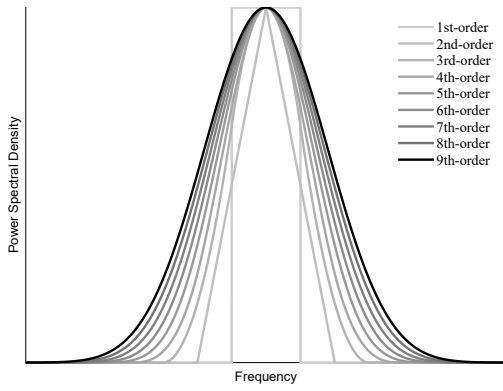
Fig. 1. Normalized envelope IMD profiles produced by a Gaussian excitation up to the 9th-order. These envelope profiles are overlapped for the sake of visualization, but they do not all overlap in the same envelope carriers. The envelope carrier frequencies for each nonlinear order are given by (3).

$$Y_{\mathrm{NL_n}}(\omega) = \mathcal{F}\{a_n x(t) \cdot x(t)^{n-1}\} = a_n \mathcal{F}\{x(t)\} * \mathcal{F}\{x(t)^{n-1}\} \quad (2)$$

As an example, let us consider a band-limited additive white Gaussian noise (AWGN) excitation signal, used in classic NPR characterization. As shown in Fig. 1, the linear envelope profile is an amplified version of the input excitation rectangular spectrum. The second-order envelope profile is triangular, resultant from the convolution of the input rectangular spectrum with itself. The remaining higher-order envelope profiles can be roughly approximated by Gaussian pulses, or by inverted parabolas when observed in logarithmic scale [22]. Note that Fig. 1 depicts the correct shape of the envelope IMD profiles, but does not represent the exact amplitude relations, as all profiles are normalized to the same peak value.

For a given order n, the full frequency response is obtained by replicating the nth-order envelope profile in each of the envelope carrier frequencies, f_{c_n}, given by (3).

$$f_{c_n} = \begin{cases} \pm f_c \cdot (2 \cdot k) & \text{if n even,} \quad k \in [0, \frac{n}{2}] \\ \pm f_c \cdot (2 \cdot k + 1) & \text{if n odd,} \quad k \in [0, \frac{n-1}{2}] \end{cases} \quad (3)$$

In (3), f_c is the fundamental carrier frequency, and $k \in N_0$.

The full static IMD response is given by the overlap of all nonlinear order responses. However, the linearity analysis is mostly concerned with inband IMD - the envelope IMD centered at f_c (co-channel frequencies + adjacent channel frequencies, as defined in [17]) - because RF systems filter out of band IMD before transmission - i.e. the envelope IMD centered around DC and high-order harmonic frequencies is typically filtered by RF transmitters. Therefore, throughout this work when referring to the IMD profile, it is meant as the inband IMD profile.

B. Static IMD Profile - Multi-Tone Excitations

In modern NPR characterization, analog noise sources were replaced by reliable digital signal generators [9], [23]. These procedures are based on equal amplitude multi-tone signals designed to resemble AWGN. Expression (4) describes a Q-tone signal.

$$x(t) = \frac{1}{2} \sum_{q=1}^{2Q} A \cdot e^{j(\omega_{\mathrm{ex}_q} t + \phi_{\mathrm{ex}_q})} \quad (4)$$

In (4), ω_{ex_q} is the q-th element of the excitation frequency vector, given by (5), and ϕ_{ex_q} is the q-th element of the excitation phase vector, given by (6).

$$\boldsymbol{\omega_{\mathrm{ex}}} = [-\omega_Q, \cdots, -\omega_1, \omega_1, \cdots, \omega_Q]^T \quad (5)$$

$$\boldsymbol{\phi_{\mathrm{ex}}} = [-\phi_Q, \cdots, -\phi_1, \phi_1, \cdots, \phi_Q]^T \quad (6)$$

For a general static nonlinear system, the nth-order response, assuming a multi-tone excitation, is given by (7). This response is obtained by inserting (4) into (1) [17], [23].

$$y_{\mathrm{NL_n}}(t) = \frac{1}{2^n} a_n \left[\sum_{q=1}^{2Q} A \cdot e^{j(\omega_{\mathrm{ex}_q} t + \phi_{\mathrm{ex}_q})} \right]^n \quad (7)$$

Using the multinomial theorem, (7) can be expressed as (8).

$$y_{\mathrm{NL_n}}(t) = \frac{1}{2^n} a_n A^n \sum_{|\boldsymbol{v}|=n} \binom{n}{\boldsymbol{v}} \prod_{q=1}^{2Q} \left[e^{j(\omega_{\mathrm{ex}_q} t + \phi_{\mathrm{ex}_q})} \right]^{v_q} \quad (8)$$

Each nth-order mixing vector, $\boldsymbol{v}$, is unique, and $\sum v_i = n$.

$$\boldsymbol{v} = [v_1, v_2, \cdots, v_{2Q}]^T; \quad v_i \in N_0 \quad (9)$$

Mixing vectors determine the IMD frequencies of each order, and weight the IMD product magnitude and phase.

The notation can be further simplified into (10).

$$y_{\mathrm{NL_n}}(t) = \boldsymbol{g} \cdot e^{j[\boldsymbol{\omega_{\mathrm{IMD}}} t + \boldsymbol{\phi_{\mathrm{IMD}}}]} \quad (10)$$

This notation is achieved by defining the nth-order mixing matrix, $\boldsymbol{V}$. This matrix contains all m nth-order mixing vectors, as expressed in (11).

$$\boldsymbol{V} = \begin{bmatrix} \boldsymbol{v_1}^T \\ \boldsymbol{v_2}^T \\ \vdots \\ \boldsymbol{v_m}^T \end{bmatrix} \quad (11)$$

In (10), $\boldsymbol{g}$ is the magnitude weighting vector, given by (12), and $\boldsymbol{\omega_{\mathrm{IMD}}} t + \boldsymbol{\phi_{\mathrm{IMD}}}$ is the IMD phase vector, given by (13).

$$\boldsymbol{g} = \frac{1}{2} a_n A^n \binom{n}{\boldsymbol{V}} = \frac{1}{2} a_n A^n \begin{bmatrix} \binom{n}{\boldsymbol{v_1}} \\ \binom{n}{\boldsymbol{v_2}} \\ \vdots \\ \binom{n}{\boldsymbol{v_m}} \end{bmatrix} \quad (12)$$

$$\boldsymbol{\omega_{\mathrm{IMD}}} t + \boldsymbol{\phi_{\mathrm{IMD}}} = [\boldsymbol{V} \cdot (\boldsymbol{\omega_{\mathrm{ex}}} t + \boldsymbol{\phi_{\mathrm{ex}}})]^T \quad (13)$$

The resulting nth-order weighting phasor, at any frequency ω, is given by the phasor sum described in (14).

$$K_n(\omega) = \sum_{i:\omega_{\mathrm{IMD}_i}=\omega} g_i \cdot e^{j\phi_{\mathrm{IMD}_i}} \quad (14)$$

$K_n(\omega)$ represents the nth-order static IMD response produced under multi-tone excitation. Therefore, the IMD frequencies generated by each nonlinear order, as well as their weight and phase, are imposed by the input multi-tone excitation and the respective mixing matrix. This means that the static IMD profile is defined by the input excitation and by the nonlinear orders of the system. Thus, if the multi-tone excitation resembles AWGN (statistically), the envelope profiles generated by each order will be discretized versions of the envelope profiles shown in Fig. 1.

It is also useful to distinguish between correlated and uncorrelated IMD weighting phasors. These can be computed using (15) and (16), respectively.

$$K_n(\omega_q)_{\text{corr}} = \sum_{i:\omega_{\text{IMD}_i}=\omega_q \ \wedge \ (V_{i,Q-q+1}\neq0 \ \vee \ V_{i,Q+q}\neq0); \ q\in[1,Q]} g_i \cdot e^{j\phi_{\text{IMD}_i}} \quad (15)$$

$$K_n(\omega_q)_{\text{uncorr}} = \sum_{i:\omega_{\text{IMD}_i}=\omega_q \ \wedge \ V_{i,\{Q-q+1,Q+q\}}=0; \ q\in[1,Q]} g_i \cdot e^{j\phi_{\text{IMD}_i}} \quad (16)$$

C. Detecting Nonlinear Dynamics

Memory observations imply a system whose response is dependent on excitation frequency. This dependence can be mathematically expressed by a deviation of the magnitude and phase weights - the g_i's and the ϕ_{IMD_i}'s in (14) - from the static IMD reference, depending on the frequency terms involved in each IMD product. Magnitude and phase variations with frequency are represented, at the system level, by frequency filters. When analyzing linearity, it is also important to distinguish linear dynamic effects [7] - the dynamic effects that affect the first-order response - from nonlinear dynamic effects - the dynamic effects that affect the static IMD profiles. Thus, the practicality of describing nonlinear dynamic systems using multi-slice models [24].

When using two-tone test signals, nonlinear dynamics can be identified though observations of IMD asymmetry, or though observations of intermodulation distortion ratio variation with carrier spacing [18], [25]. However, in a multi-tone scenario the observation of these features is not a sufficient condition for the detection of nonlinear dynamics, as already noted in [18]. As far as the authors' knowledge goes, a systematic way to detect nonlinear dynamic effects from IMD profile observations under multi-tone excitation has not yet been presented in the literature. Meanwhile, the aforementioned qualitative criteria based on the 2-tone scenario continue to be used to detect nonlinear dynamics under multi-tone excitation [19], [20].

Note that the theoretical tools presented provide sufficient insight to address this issue. In Section II-B it was shown that the static IMD profile is imposed by the input multi-tone excitation, and by the system nonlinear order. As mentioned, nonlinear dynamics filter the static IMD profile, changing $K_n(\omega)$. Thus, for a given multi-tone excitation, nonlinear dynamics should be gauged as the error between the measured dynamic IMD profile and the static reference IMD profile. This approach can be viewed as an extension of the memory metric, proposed in [25] for the 2-tone excitation, to the multi-tone

excitation scenario for systems of any nonlinear order. One advantage of this solution over the one presented in [18] is that it does not impose limitations on the multi-tone excitation characteristics.

In fact, it is the specification of the static reference response in agreement with the input excitation that allows the notion of expected IMD response, which, as a consequence, allows the detection of nonlinear dynamics. This becomes evident by transposing the classic analysis, presented in [18], to the system-level. It uses an equal magnitude 2-tone excitation, and assumes a third-order system. By computing the static third-order weighting phasor in these conditions, using (14), one IMD product falls in the lower adjacent channel, one IMD product falls in the upper adjacent channel, and these IMD products have the same weight. This implies that a memoryless system must have a flat adjacent-channel IMD response. Therefore, adjacent channel IMD asymmetry and adjacent channel IMD variation with carrier spacing become indicators of nonlinear dynamic effects. It is the understanding of the reference that gives meaning to the IMD profile analysis!

For systems of any order under multi-tone excitation, it is difficult to intuitively guess the static reference IMD profile because many IMD phasors overlap at inband IMD frequencies, as also expressed in (14). Despite this, expected IMD responses are often assumed without computing the reference [5], [7], [19], [20], [21]. This imposes important limitations on the IMD profile analysis. One is that it is not possible to do objective comparisons, and qualitative observations might not be rigorous. Another one is that small changes in the input signal characteristics can affect the reference, therefore, not computing the reference can lead to erroneous considerations. This is most problematic when the experimental setup is compensated, or the experimental results are processed, based on incorrect assumptions about the IMD response. Thus, the importance of specifying the static IMD reference response under multi-tone excitation when evaluating nonlinear dynamics, as proposed here.

III. CLASSIC NONLINEAR DYNAMIC RF MECHANISM

When addressing nonlinear dynamic RF systems, the classic mechanism, first explained in [18], is often assumed. To complement the circuit-level analysis presented in [18], this section presents an in-depth system-level analysis, focused on the IMD profile response under multi-tone excitation.

The classic nonlinear dynamic mechanism is depicted in the schematic of Fig. 2. It consists of a static nonlinear branch and a nonlinear dynamic branch. These two branches add, interfering with each other, to produce the resultant output envelope IMD profile.

The static nonlinear branch consists of a third-order nonlinearity. Thus, the static branch IMD profile contribution is directly computed from (14), substituting for third-order.

The nonlinear dynamic branch consists of a second-order nonlinearity that is filtered before being remixed with the input signal. It can be viewed as a special case of a dynamic third-order nonlinearity in which IMD is filtered at baseband and second-harmonic before manifesting at the fundamental
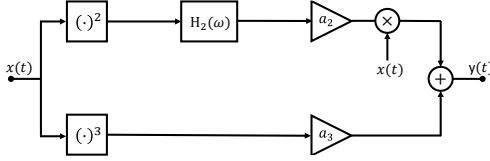
Fig. 2. Classic nonlinear dynamic mechanism model. This model addresses nonlinear dynamics (the linear path is omitted).

and third-harmonic frequencies. If not for $H_2(\omega)$, this branch would also constitute a static third-order nonlinearity. To understand the contribution of the nonlinear dynamic branch to the resultant envelope IMD profile, we must know exactly how second-order IMD products convert to third-order IMD frequencies in this branch. To do that, let us first neglect the impacts of $H_2(\omega)$ and address only the nonlinear conversion.

From (7), it is possible to decompose any nonlinearity of order n as the product of a nonlinearity of order n-1 with the input excitation, as shown in (17).

$$y_{\mathrm{NL}_n}(t) = a_n \; x(t)^{n-1} \cdot x(t) \qquad (17)$$

Thus, the static conversion of a second-order nonlinearity to a third-order nonlinearity is mathematically described by (18).

$$y_{\mathrm{NL}_3}(t) = \frac{a_3}{a_2} \cdot y_{\mathrm{NL}_2}(t) \cdot \frac{1}{2} \cdot A \cdot \sum_{q=1}^{2Q} e^{j(\omega_{\mathrm{ex}_q} t + \phi_{\mathrm{ex}_q})} \qquad (18)$$

Note that each second-order IMD frequency, ω_{IMD_2}, converts to the third-order IMD frequency $\omega_{\mathrm{IMD}_2} + \omega_{ex_q}$. Therefore, the conversion gain, given by (19), can be derived from (14).

$$K_3(\omega_{\mathrm{IMD}_3}) = \frac{a_3}{a_2} \frac{1}{2} A \sum_{\forall \omega_{\mathrm{IMD}_2} + \omega_{\mathrm{ex}_q} = \omega_{\mathrm{IMD}_3}; \; q \in [1, 2Q]} K_2(\omega_{\mathrm{IMD}_2}) \cdot e^{j\phi_{\mathrm{ex}_q}} \qquad (19)$$

Equation (19) establishes the phasor relationship between static second-order IMD profiles and static third-order IMD profiles. $H_2(\omega)$ affects the magnitude and phase of each second-order IMD product, captured in $K_2(\omega_{\mathrm{IMD}_2})$. This ultimately deviates the nonlinear dynamic branch IMD profile from the static third-order IMD profile.

Therefore, the sum of the static and dynamic branches, that produces the resultant IMD profile, is a phasor sum at every third-order IMD frequency. This means that, when analyzing the classic nonlinear dynamic mechanism at the system-level under multi-tone excitation, the nonlinear dynamics introduced by $H_2(\omega)$ should be gauged as the error between the resultant IMD profile and the static third-order IMD reference profile.

IV. DYNAMIC IMD PROFILES - EXAMPLE ANALYSIS

This section analyses distinct examples of dynamic IMD profiles produced by the classic nonlinear dynamic RF mechanism. These examples serve the following purposes:

1) to validate numerically the presented theory;
2) to emphasize the need for a static reference to make sense of IMD profiles;
3) to evidence the limitations of classic multi-tone linearity metrics in the presence of nonlinear dynamic effects.

Before the example analysis, the example systems, the input stimulus, the IMD reference profile, and the computation method are presented to parameterize the numerical examples.

A. Example Systems

As stated, all examples follow the block diagram of the classic nonlinear dynamic system, depicted in Fig. 2.

For the sake of simplicity, all the static gains, a_2 and a_3, are normalized to 1, and only the filter structure, $H_2(\omega)$, is varied. Three examples are considered for analysis. The $H_2(\omega)$ filters of examples I, II and III are described in Table. I, Table. II, and Table. III, respectively.

B. Input Stimulus

In this example analysis, the input stimulus is an equal magnitude 5-tone excitation, equally spaced and phase aligned. The amplitude, A from (4), is normalized to 1.

Note that this is not a standard NPR excitation. The NPR excitation has higher number of tones - i.e. higher frequency domain resolution - and the tone phases are designed to mimic band-limited AWGN statistical characteristics. This input stimulus simplification is done for the sake of intelligibility of the numerical examples, without loss of generality.

The validity of this approach is provided from (8) to (14). Note that varying the number of tones changes the the mixing matrix, thus varying the number of IMD frequencies generated, as expressed in (13). Also, tone phase manipulations change the weight phasor sum at each IMD frequency, as expressed in (14). Thus, changing multi-tone excitation parameters changes the domains of analysis - IMD frequency and IMD power - but this does not impact the analysis tools presented, as long as the IMD reference profile is defined in agreement with the input multi-tone excitation.

C. IMD Reference Profile

As mentioned in Section III, the reference for the classic mechanism is a static third-order IMD profile. But before computing the reference, the IMD frequency domain of analysis has to be specified in agreement with the input multi-tone excitation.

For equally spaced tones, the adjacent channel expands

$$\pm \frac{n-1}{2} \cdot (N_{\mathrm{tones}} - 1) \cdot \Delta f \qquad (20)$$

beyond the co-channel. Where n can be any odd-order, N_{tones} is the number of excitation tones, and Δf is the carrier spacing. Equation (20) can be derived from (13).

Therefore, for the 5-tone input stimulus, the third-order IMD reference profile ranges from $\omega_1 - 4\Delta f$ to $\omega_5 + 4\Delta f$. Given this information, the IMD reference profile is computed at the interest IMD frequencies from (14), substituting for third-order with a_3 normalized to 1. The IMD reference profile is listed in Table. IV and depicted in Fig. 3.

Here it is assumed that the lowest IMD frequency is higher than DC. It is also assumed that third-order IMD envelope

TABLE I
$H_2(\omega)$ FILTER OF EXAMPLE 1.

$H_2(\omega)$	$-4\Delta f$	$-3\Delta f$	$-2\Delta f$	$-\Delta f$	REF	Δf	$2\Delta f$	$3\Delta f$	$4\Delta f$
$|H_2(\omega)|$	1	1	0.75	0.75	0.75	0.75	0.75	1	1
$\angle H_2(\omega)$	0	0	π	π	π	π	π	0	0

TABLE II
$H_2(\omega)$ FILTER OF EXAMPLE 2.

$H_2(\omega)$	$-4\Delta f$	$-3\Delta f$	$-2\Delta f$	$-\Delta f$	REF	Δf	$2\Delta f$	$3\Delta f$	$4\Delta f$
$|H_2(\omega)|$	1	1	1	1	1	1	1	1	1
$\angle H_2(\omega)$	0	0	0	π	π	π	0	0	0

TABLE III
$H_2(\omega)$ FILTER OF EXAMPLE 3.

$H_2(\omega)$	$-4\Delta f$	$-3\Delta f$	$-2\Delta f$	$-\Delta f$	REF	Δf	$2\Delta f$	$3\Delta f$	$4\Delta f$
$|H_2(\omega)|$	1	1	1	1	1	1	1	1	1
$\angle H_2(DC)$	π	π	π	π	0	π	π	π	π
$\angle H_2(2\omega_3)$	π	π	π	π	π	0	0	0	0

TABLE IV
REFERENCE FUNDAMENTAL ENVELOPE STATIC THIRD-ORDER PROFILE - 5-TONE EXCITATION

$\omega_1 - 4\Delta f$	$\omega_1 - 3\Delta f$	$\omega_1 - 2\Delta f$	$\omega_1 - 1\Delta f$	ω_1	ω_2	ω_3	ω_4	ω_5	$\omega_5 + 1\Delta f$	$\omega_5 + 2\Delta f$	$\omega_5 + 3\Delta f$	$\omega_5 + 4\Delta f$
0.375	1.125	2.25	3.75	5.625	6.75	7.125	6.75	5.625	3.75	2.25	1.125	0.375

profiles centered at the fundamental and at the third-harmonic frequencies do not overlap. Such assumptions avoid image channel overlap, which simplify the example analysis. Note, however, that the theoretical tools presented are also valid in such scenarios. In case of image channel overlap, the third-order IMD reference profile differs from the one presented here, in accordance to the specific scenario.

D. Classic Mechanism - Numerical Computation Method

As explained in Section III, the classic mechanism IMD profile is given by the phasor sum of the IMD profiles produced by the static and dynamic branches. Therefore, the IMD profile numerical computation starts by the independent computation the IMD profiles imposed by each branch.

The static branch is a third-order nonlinearity. Thus, the static branch IMD profile is given by the reference IMD profile, as explained in Section IV-C.

The dynamic branch performs a frequency conversion from second-order IMD frequencies to third-order IMD frequencies. So, before computing the IMD profile, the conversion domain has to be specified in agreement with the 5-tone input stimulus. As noted in IV-C, the third-order IMD profile ranges from $\omega_1 - 4\Delta f$ to $\omega_5 + 4\Delta f$. Around DC, second-order IMD ranges from $-4\Delta f$ to $+4\Delta f$. Around the second harmonic, second-order IMD ranges from $2\omega_3 - 4\Delta f$ to $2\omega_3 + 4\Delta f$. Note that second-order IMD frequencies are computed from (13).

After specifying the conversion domain, the conversion gain of each IMD product is computed from (19). Table. V lists the static conversion gain from DC, whereas Table. VI lists the

static conversion gain from the second harmonic. As expected, these conversions differ by a factor of 2.

The dynamic effects, introduced by $H_2(\omega)$, are computed by scaling the static conversion gain tables - Table. V and Table. VI - at each second-order IMD frequency. The scaling factor is the phasor response of $H_2(\omega)$ at each IMD frequency.

At this point, the dynamic branch IMD profile is computed in two steps. First, add Table. V and Table. VI after applying $H_2(\omega)$ filtering. Second, compute the line element sum of the resulting table. For a memoryless conversion, the dynamic branch IMD profile coincides with the reference, as expected.

Finally, the classic mechanism IMD profile is given by the sum of the static branch IMD profile and dynamic branch IMD profile. For a memoryless conversion, this also coincides with the reference, amplified by 3 dB, as expected.

E. Example Analysis

The IMD profiles produced by each numerical example, computed as described in Section IV-D, are depicted in Fig. 3.

These IMD profiles present rather unusual trends. Example I presents a co-channel IMD minimum at the central frequency, instead of a IMD maximum. Example II presents co-channel IMD oscillation, having equal power at the start, middle and end of the band, while having lower power at intermediate frequencies ω_2 and ω_4. Example III presents strong adjacent channel asymmetry, and co-channel IMD power increases monotonically along the co-channel.

However, one must remember that IMD profile trends alone do not objectively inform about nonlinear dynamics. The meter

TABLE V
STATIC CONVERSION TABLE FROM DC TO FUNDAMENTAL FOR THE 5 TONE INPUT STIMULUS

	$DC - 4\Delta f$	$DC - 3\Delta f$	$DC - 2\Delta f$	$DC - \Delta f$	DC	$DC + \Delta f$	$DC + 2\Delta f$	$DC + 3\Delta f$	$DC + 4\Delta f$
$\omega_1 - 4\Delta f$	0.25	0	0	0	0	0	0	0	0
$\omega_1 - 3\Delta f$	0.25	0.5	0	0	0	0	0	0	0
$\omega_1 - 2\Delta f$	0.25	0.5	0.75	0	0	0	0	0	0
$\omega_1 - \Delta f$	0.25	0.5	0.75	1	0	0	0	0	0
ω_1	0.25	0.5	0.75	1	1.25	0	0	0	0
ω_2	0	0.5	0.75	1	1.25	1	0	0	0
ω_3	0	0	0.75	1	1.25	1	0.75	0	0
ω_4	0	0	0	1	1.25	1	0.75	0.5	0
ω_5	0	0	0	0	1.25	1	0.75	0.5	0.25
$\omega_5 + \Delta f$	0	0	0	0	0	1	0.75	0.5	0.25
$\omega_5 + 2\Delta f$	0	0	0	0	0	0	0.75	0.5	0.25
$\omega_5 + 3\Delta f$	0	0	0	0	0	0	0	0.5	0.25
$\omega_5 + 4\Delta f$	0	0	0	0	0	0	0	0	0.25

TABLE VI
STATIC CONVERSION TABLE FROM SECOND HARMONIC TO FUNDAMENTAL FOR THE 5 TONE INPUT STIMULUS

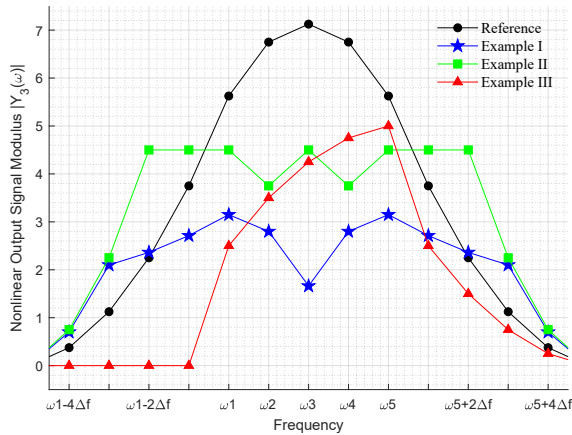|	$2\omega_3 - 4\Delta f$	$2\omega_3 - 3\Delta f$	$2\omega_3 - 2\Delta f$	$2\omega_3 - \Delta f$	$2\omega_3$	$2\omega_3 + \Delta f$	$2\omega_3 + 2\Delta f$	$2\omega_3 + 3\Delta f$	$2\omega_3 + 4\Delta f$
$\omega_1 - 4\Delta f$	0.125	0	0	0	0	0	0	0	0
$\omega_1 - 3\Delta f$	0.125	0.25	0	0	0	0	0	0	0
$\omega_1 - 2\Delta f$	0.125	0.25	0.375	0	0	0	0	0	0
$\omega_1 - \Delta f$	0.125	0.25	0.375	0.5	0	0	0	0	0
ω_1	0.125	0.25	0.375	0.5	0.625	0	0	0	0
ω_2	0	0.25	0.375	0.5	0.625	0.5	0	0	0
ω_3	0	0	0.375	0.5	0.625	0.5	0.375	0	0
ω_4	0	0	0	0.5	0.625	0.5	0.375	0.25	0
ω_5	0	0	0	0	0.625	0.5	0.375	0.25	0.125
$\omega_5 + \Delta f$	0	0	0	0	0	0.5	0.375	0.25	0.125
$\omega_5 + 2\Delta f$	0	0	0	0	0	0	0.375	0.25	0.125
$\omega_5 + 3\Delta f$	0	0	0	0	0	0	0	0.25	0.125
$\omega_5 + 4\Delta f$	0	0	0	0	0	0	0	0	0.125

Fig. 3. IMD profiles obtained through numerical simulation: static reference and nonlinear dynamic examples.
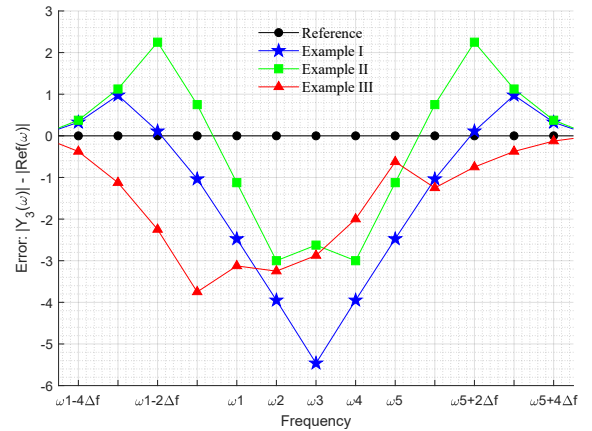

Fig. 4. IMD profile error. Positive error indicates IMD above the static reference. Negative error indicates IMD bellow the static reference.

for nonlinear dynamic quantification is the frequency dependence of the error between the IMD profile and reference, not the IMD profile trend. As shown in Fig. 4, this error is frequency dependent for each example, confirming the presence of nonlinear dynamics. Note how these are good examples of how distinct the impacts of nonlinear dynamics on the IMD profile can be. For instance, Example I and Example II expose the limitations of expecting nonlinear dynamics to manifest

TABLE VII
IMD POWER EVALUATION USING CLASSIC LINEARITY METRICS

Metric	ACP_L	ACP_U	NP	CCP
Reference	20.5	20.5	50.8	205.2
Example I	19.5	19.5	2.0	36.5
Example II	46.1	46.1	20.1	88.9
Example III	0.0	9.1	18.1	84.1

Fig. 5. Third-order dynamic nonlinear system model. This model addresses nonlinear dynamics, thus the linear path is not presented.

through asymmetric IMD profiles/asymmetric errors.

These examples also expose the limitations of classic multi-tone linearity metrics, such as ACPR, NPR and CCPR, in the assessment of nonlinear memory effects. Note that these metrics cannot quantify nonlinear dynamics, because they do not specify a static reference in accordance with the input stimulus. Beyond this, even if a reference is postulated, the integrals, explicit in the definition of these metrics [26], hide the frequency dependence of the IMD response. Thus, these metrics cannot gauge the frequency dependence of the error between measurement and reference IMD profiles, they can only gauge the difference between measured and reference IMD power within the evaluation bandwidth. This power error can incorrectly account a frequency independent error as nonlinear dynamics. It can also mask nonlinear dynamics whenever these do not translate into total IMD power errors within the evaluation bandwidth. This means that these metrics, in their classical formulation, lack frequency resolution to accurately evaluate nonlinear dynamics.

To evidence how relevant information regarding nonlinear dynamics is lost in classic linearity metrics, IMD power, as evaluated by ACPR, CCPR and NPR, is listed in Table. VII. ACP_L denotes the IMD power sum from $\omega_1 - 4\Delta f$ to $\omega_1 - \Delta f$, as evaluated by ACPR_L. ACP_U denotes the IMD power sum from $\omega_1 + \Delta f$ to $\omega_1 + 4\Delta f$, as evaluated by ACPR_U. NP denotes the IMD power at ω_3, as evaluated by a classic NPR measurement with a central notch. CCP denotes the IMD power sum from ω_1 to ω_5, as evaluated by CCPR. Note that IMD power is adimensional because the numerical example signals are adimensional.

Consider the ACP. In Example III the ACP measure detects not only the presence of nonlinear dynamic effects in the L-band and in the U-band, but it is also capable of detecting the large error difference between the L-band and the U-band. However, in Example I the ACP error is too marginal to confidently detect the existing nonlinear dynamic effects. Beyond this, the perception of the IMD frequencies in which IMD power is above or bellow the reference, as observed in Fig. 4, is lost. This happens because the coarse ACP analysis loses the frequency resolution required to detect these features imposed by nonlinear dynamic effects. It is no longer possible to relate IMD power to specific IMD frequency bands. Also, observe how ACP is not indicative of the CCP, and vice-versa.

NP detects the absolute IMD error at the central frequency, ω_3, but it is not indicative of the error variations that occur at other co-channel frequencies. Observe that Example II and Example III have similar NP, but these examples manifest very distinct co-channel IMD profiles (refer to Fig. 3 and
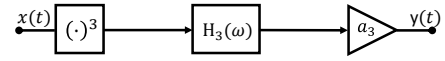
Fig. 4). This evidences the importance of using swept-notch NPR measurements [21].

The use of CCP does not necessarily provide a better insight than NP. As already explained, Example II IMD power oscillates along the co-channel, whereas Example III IMD power monotonically increases along the co-channel. The CCP coarse analysis does not have sufficient frequency resolution to appropriately capture these variations imposed by nonlinear dynamic effects. This is the reason why CCP indicates similar IMD power levels for both scenarios.

The presented analysis indicates that a reliable characterization of IMD profiles affected by nonlinear dynamic effects requires the measurement of both adjacent-channel and co-channel IMD, with sufficient resolution frequency. Then, the analysis of the measured IMD profile has to be performed in relation to the static IMD reference profile.

V. LIMITATIONS OF MECHANIM BASED IMD ANALYSIS

As stated in Section III, in RF systems the IMD analysis is often performed assuming the classic nonlinear dynamic mechanism. However, IMD analysis based on specific mechanisms have strong limitations in terms of range of applicability. If the system under test differs from the analysis mechanism, the analysis is no longer valid. An obvious limitation of the classic mechanism is that it is strongly bound to third-order nonlinearity.

Range of applicability limitations directly translate into experimental setups and procedures in which specific nonlinear mechanisms are assumed prior to measurement. Studies [7] and [19] are good examples of nonlinear characterization based on specific mechanisms. When following this approach, one must be careful, because whenever incorrect assumptions are made in experiments, these translate into errors in the experimental results.

The limitations of mechanism based IMD analysis span beyond the nonlinear order of the system, because different systems, of equal nonlinear order, can produce the same response for a given excitation. Remember, from Section III, that a static second-order nonlinearity up-converted to third-order is indistinguishable from a static third-order nonlinearity. In fact, it is a static third-order nonlinearity. Beyond this, it is possible to have a different third-order system that produces the IMD profiles generated by the classic mechanism in Section IV-E, for the same excitation signal.

Consider the third-order nonlinear dynamic mechanism depicted in Fig. 5. It consists of a static third-order nonlinearity followed by a filter, $H_3(\omega)$. The static nonlinear contribution is given by (14), substituting for third-order. The filter, $H_3(\omega)$, affects the magnitude and phase of each IMD product captured in $K_3(\omega)$. For the example scenario described in Section IV, the static third-order contribution is given by the

IMD reference profile, after normalizing a_3 to 1. The dynamic effects, introduced by $H_3(\omega)$, scale the IMD reference profile. The scaling factor is the phasor response of $H_3(\omega)$ at each third-order IMD frequency. Thus, this mechanism can produce exactly the IMD profiles shown in Fig. 3, for the same excitation, if $H_3(\omega)$ is given by the normalization of the example IMD profiles by the static IMD reference profile. Table. VIII, Table. IX, and Table. X list the $H_3(\omega)$ filters, obtained through normalization, that produce the IMD profiles of Example I, Example II, and Example III, respectively.

Therefore, general experimental setups and procedures must avoid making assumptions about the nonlinear dynamic mechanism of the system under test. Such considerations must be made based on the analysis of unbiased experimental results. Specific experimental setups and procedures should only be used when there is prior knowledge about the system, and there is a need for a tailored characterization.

VI. NONLINEAR DYNAMIC RF SYSTEM CHARACTERIZATION

So far, the presented work brought important insights into the analysis of the IMD response produced by nonlinear dynamic RF systems, exposing relevant limitations of existing linearity metrics on the quantification of nonlinear dynamics.

This section reframes those insights from a characterization perspective, summarizing the major contributions of this work in a way that they can be instrumentally used to improve characterization techniques, and linearity metrics, on the assessment of nonlinear dynamics.

Beyond this, these contributions are used to propose a novel characterization procedure that overcomes the most critical limitations of standard procedures.

A. General Guidelines for Procedures and Metrics

The major contributions already presented can be summarized in a list of general guidelines for more reliable experimental procedures and linearity metrics, as follows:

1) Specify a static IMD reference profile in agreement with the input excitation: It was shown that IMD profiles are highly dependent on the input excitation. The definition of a reference avoids the misinterpretation of the experimental results. Beyond this, nonlinear dynamics are detected through the frequency dependence of the error between measured IMD profile and IMD reference;

2) Avoid blind mechanism based characterization: It was explained that mechanism based characterization has a very restrictive range of validity, and that incorrect assumptions can lead to experimental errors. Instead of blindly assuming a nonlinear dynamic mechanism, start from unbiased experimental results before moving to a mechanism based analysis;

3) Perform full inband IMD characterization: It was shown that in the presence of nonlinear dynamics, adjacent-channel IMD trends are not necessarily indicative of co-channel IMD trends, and vice-versa. Capturing both adjacent-channel and co-channel IMD allows for a more comprehensive understanding of the nonlinear dynamic mechanism being characterized;

4) Perform magnitude and phase measurements: The theoretical formulation evidences that important information about system dynamics is concealed in the phase of the overlapping IMD products at each IMD frequency. Therefore, magnitude and phase measurements are preferred over power measurements;

5) Use frequency dependent linearity metrics: It was demonstrated that informative linearity metrics must capture the frequency dependence of the measured IMD profile in relation to the reference with sufficient frequency resolution.

B. Swept-Tone NPR

Given the aforementioned guidelines, this section proposes a reliable characterization method, based on classic NPR procedures, to measure IMD profile responses produced by nonlinear dynamic RF systems.

First, the input stimulus has to be specified. For the swept-tone NPR the input excitation can be any equal amplitude multi-tone signal, with equally spaced tones. For those signals, the full inband response is given by (21), where $K_{n_d}(\omega)$ is the dynamic weighting phasor of order n, observed at the system output. It results from the static weighting phasor, given by (14), being filtered by the system memory effects.

$$\sum_{n=0}^{\infty} K_{n_d}(\omega) \quad , \quad \omega \in \text{inband} \tag{21}$$

From (15) and (16), this inband IMD response can be decomposed in correlated IMD and uncorrelated IMD components, as expressed in (22).

$$\sum_{n=0}^{\infty} K_{n_d}(\omega) = \sum_{n=0}^{\infty} K_{n_d}(\omega)_{\text{corr}} + \sum_{n=0}^{\infty} K_{n_d}(\omega)_{\text{uncorr}} \tag{22}$$

In RF systems the desired response is the correlated response, because correlated IMD components can be used to regenerate communication signals at the receiver [4], [16]. Thus, from an RF system perspective, the uncorrelated IMD response is the interest nonlinear response to be measured.

From a characterization perspective, the full inband response, given by (21), is measured with a full spectrum multi-tone excitation. This measurement fully captures the adjacent-channel portion of the uncorrelated nonlinear envelope response, but overlaps correlated and uncorrelated responses at the co-channel frequencies.

From (15) and (16), it is perceptible that if a single excitation tone, ω_{off}, is turned off, all IMD phasors correlated with the ω_{off} excitation phasor are also switched off, but all uncorrelated phasors that fall in ω_{off} are preserved. Thus, the co-channel uncorrelated IMD response can be measured by switching off a single excitation tone, taking a measurement, recording the uncorrelated IMD at the switched off excitation frequency, sweeping the switched off tone along the co-channel, and repeating this process until all excitation frequencies are characterized in terms of uncorrelated IMD. To illustrate this procedure, the swept-tone NPR excitation signals, for a 5-tone input stimulus, are shown in Fig. 6.

TABLE VIII
$H_3(\omega)$ FILTER THAT PRODUCES EXAMPLE 1 RESPONSE FOR THE THIRD-ORDER DYNAMIC NONLINEAR CASE

$H_3(\omega)$	$-6\Delta f$	$-5\Delta f$	$-4\Delta f$	$-3\Delta f$	$-2\Delta f$	$-\Delta f$	REF	Δf	$2\Delta f$	$3\Delta f$	$4\Delta f$	$5\Delta f$	$6\Delta f$
$|H_3(\omega)|$	2	2	1.1	0.74	0.56	0.4	0.2	0.4	0.56	0.74	1.1	2	2
$\angle H_3(\omega)$	0	0	0	0	0	0	0	0	0	0	0	0	0

TABLE IX
$H_3(\omega)$ FILTER THAT PRODUCES EXAMPLE 2 RESPONSE FOR THE THIRD-ORDER DYNAMIC NONLINEAR CASE

$H_3(\omega)$	$-6\Delta f$	$-5\Delta f$	$-4\Delta f$	$-3\Delta f$	$-2\Delta f$	$-\Delta f$	REF	Δf	$2\Delta f$	$3\Delta f$	$4\Delta f$	$5\Delta f$	$6\Delta f$
$|H_3(\omega)|$	2	2	2	1.2	0.8	$\frac{5}{9}$	$\frac{12}{19}$	$\frac{5}{9}$	0.8	1.2	2	2	2
$\angle H_3(\omega)$	0	0	0	0	0	0	0	0	0	0	0	0	0

TABLE X
$H_3(\omega)$ FILTER THAT PRODUCES EXAMPLE 3 RESPONSE FOR THE THIRD-ORDER DYNAMIC NONLINEAR CASE

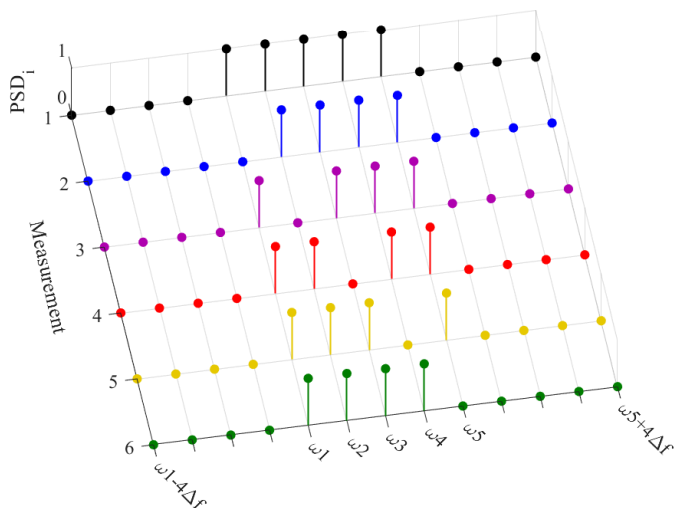| $H_3(\omega)$	$-6\Delta f$	$-5\Delta f$	$-4\Delta f$	$-3\Delta f$	$-2\Delta f$	$-\Delta f$	REF	Δf	$2\Delta f$	$3\Delta f$	$4\Delta f$	$5\Delta f$	$6\Delta f$
$|H_3(\omega)|$	0	0	0	0	$\frac{4}{9}$	$\frac{14}{27}$	$\frac{34}{57}$	$\frac{19}{27}$	$\frac{8}{9}$	$\frac{2}{3}$	$\frac{2}{3}$	$\frac{2}{3}$	$\frac{2}{3}$
$\angle H_3(\omega)$	0	0	0	0	0	0	0	0	0	0	0	0	0

Fig. 6. Swept-tone notch NPR excitation signals PSD, assuming a 5-tone excitation.

The aforementioned measurements characterize the full in-band response and the uncorrelated inband response. These measurements allow for the computation of the correlated inband response through (22), by subtracting the uncorrelated inband response from the full inband response.

It is now important to define the static reference IMD envelope profile. One approach to define the static reference is to use system input/output observations. With the full spectrum multi-tone excitation input/output observations, the best static model can be computed in a least squares sense [25], [26]. Then, the swept-tone NPR excitations can be applied to this model to compute the co-channel uncorrelated IMD response. With this, the best static reference IMD profile can be defined. Note that in this process no assumptions are made about the system, and no processing is done on the experimental results. But assumptions are made about the static reference, which instead of capturing the real a_n values from (1), it optimizes the a_n values to minimize error in the least squares sense. This means that deviations of the measured uncorrelated IMD profile from the static reference uncorrelated IMD profile are measures of the minimum dynamic deviations, not absolute deviation measures.

Lets finally address the linearity metrics. When evaluating linearity it continues to be important to measure the signal to noise distortion ratio (SNDR), as postulated in classic linearity metrics. In the proposed method this can be easily evaluated by (23).

$$SNDR = \frac{\text{Correlated Power}}{\text{Uncorrelated Power}} \quad (23)$$

Following the formulation in (22), the correlated power is given the commutative power of the correlated inband response spectrum - linear power + correlated IMD power - whereas the uncorrelated power is given the commutative power of the uncorrelated inband response spectrum - adjacent-channel uncorrelated IMD power + co-channel uncorrelated IMD power. These powers are directly obtained by computing the cumulative power of the correlated inband response and the uncorrelated inband response, respectively, which are measured as explained above.

However, system nonlinear dynamics cannot be neglected. To capture nonlinear dynamics, the SNDR measure has to be accompanied by the uncorrelated IMD profile and the reference IMD profile. The error between these profiles quantifies the variations due to nonlinear dynamic effects. These profiles can also be presented in relation to the correlated power, thus expressing the SNDR variation along the adjacent channel and co-channel. Note how this overcomes the aforementioned limitations of ACPR, NPR and CCPR.

The full characterization method proposed is summarized in the flowchart of Fig. 7.

To speed up characterization in a practical application scenario, the experimental procedure can be simplified by swiping a small bandwidth notch instead of a single tone
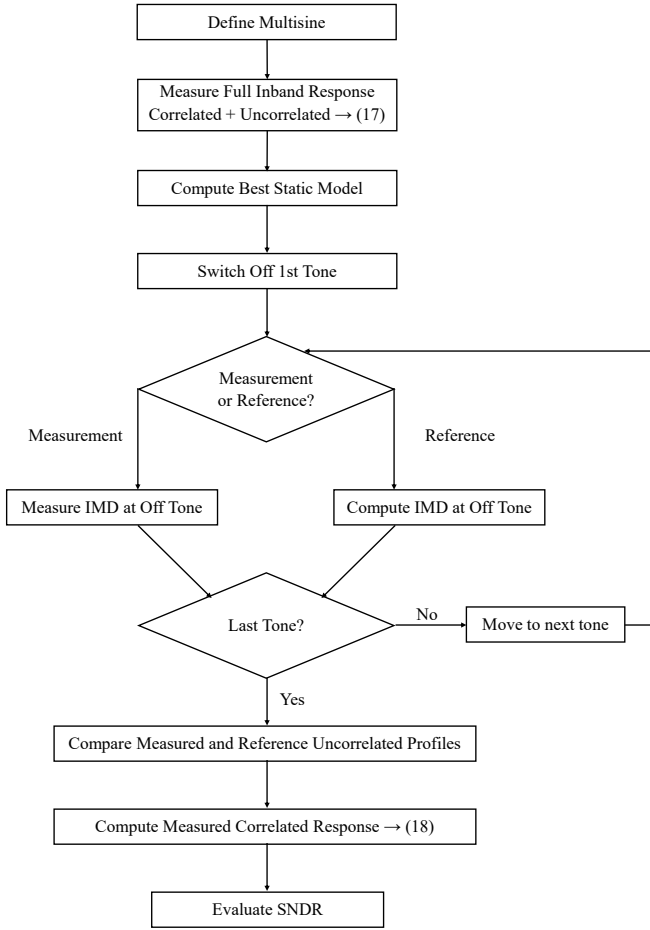
(a) Setup Schematic.
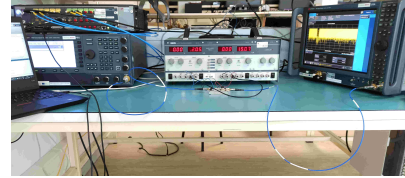
(b) Setup Picture.
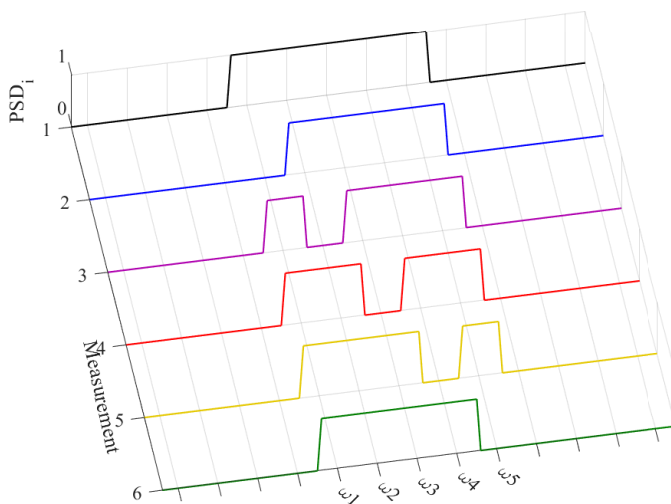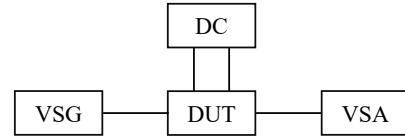
Fig. 9. Experimental Setup.

notch, as proposed in [21]. The swept-notch NPR exitation signals for such a scenario are shown in Fig. 8. The IMD profile observations using this method are valid as long as the system is slowly varying along the co-channel, when compared to the notch bandwidth, i.e. as long as the notch provides sufficient frequency resolution to capture the existing nonlinear dynamic effects. Note, however, that this modification does not allow for the computation of the correlated response as previously formulated in (22).

VII. EXPERIMENTAL VALIDATION

The main objective of this section is to validate the theoretical contributions of this work experimentally. Namely, evidencing the limitations of classical metrics - ACPR, NPR and CCPR - in the assessment of nonlinear dynamics, and evidencing the usefulness of the general characterization guidelines proposed to overcome those limitations. This is achieved by comparing the IMD profile obtained from the proposed swept-tone NPR procedure with IMD power measures obtained from classical procedures.

Before advancing into the experimental result analysis, the swept-tone NPR experimental validation is described in terms of experimental setup, input stimulus, and devices-under-test (DUTs).

A. Experimental Setup

The experimental setup is designed and configured to perform the swept-tone NPR procedure described in Fig. 7.

The experimental bench is depicted in Fig. 9. The VSG is composed of a Keysight M8190A AWG and a Keysight E8361C PSG. The AWG is used to generate the desired input baseband I/Q waveform, whereas the PSG serves to up-convert this baseband waveform to the desired carrier frequency, while controlling the envelope signal power. The Keysight N9041B UXA VSA function is to capture the input/output I/Q waveforms. The TTI PL330DP DC supply is used to bias the DUTs.

The DC supply is controlled manually, whereas the VSG and VSA equipments are remotely controlled to follow the procedure depicted in Fig. 7 closely. The bench is calibrated to capture the desired I/Q waveforms synchronously at the input and output ports.

Fig. 7. Characterization method flowchart.

Fig. 8. Swept notch NPR excitation signals PSD, proposed in [21].

B. Input Stimulus

As explained in Section VI-B, the swept-tone NPR specifies the input excitation as any equal amplitude multi-tone signal, with equally spaced tones. Before experimentation, this signal has to be parameterized in power level, bandwidth and number of tones. Note that the specification of bandwidth and the number of tones imposes the carrier spacing, which is the resolution frequency of the swept-tone NPR procedure.

During the experiments, signal power and signal bandwidth were fixed at -10 dBm and 100 MHz, respectively, whereas the number of tones was varied. Two input stimulus were used, one with 5-tones and another with 101-tones. In other words, one with 25 MHz resolution frequency and another with 1 MHz resolution frequency.

The 5-tone signal has phase aligned tones. This signal is similar to the one used for theoretical exemplification, which allows a familiar transition from the theoretical analysis to the experimental analysis. The idea is to show that signals with these characteristics can also be used to measure IMD and nonlinear dynamics in practical scenarios.

The 101-tone excitation has randomized phases, designed following the guidelines presented in [27] to resemble AWGN. This signal corresponds to a typical NPR characterization signal. The idea is to show that the presented concepts also apply to characterization signals used for the evaluation of classic linearity metrics.

C. Devices Under Test

During the experimental procedure, two devices were characterized: an Era-2+ [28], and a ZVA-213-S+ [29].

The Era-2+ is a stable off-the-shelf device known to be memoryless. It is used to validate the static reference IMD profile extraction procedure followed in swept-tone NPR characterization. The Era-2+ board operates from 5.55 GHz to 5.75 GHz, having a $P_{1_{dB}}$ of 11 dBm. It is biased with 8.4 V, consuming 50 mA. It is excited at a 5.67 GHz carrier. For the input-stimulus with -10 dBm input power, it outputs an envelope power of 1 dBm, which is in agreement with the typical gain of 10.7 dB.

The ZVA-213-S+ is a wideband amplifier of interest for Ku-band radar and satellite applications. Its large operation bandwidth is an indicator for the manifestation of nonlinear dynamic effects. This device is used to validate the ability of swept-tone NPR to gauge nonlinear dynamics. The ZVA-213-S+ board operates from 800 MHz to 21 GHz, having a $P_{1_{dB}}$ of 24 dBm. It is biased with 12 V, consuming 340 mA. It is excited at an 18 GHz carrier. For the input-stimulus with -10 dBm input power, it outputs an envelope power of 15.6 dBm, which is in agreement with the typical gain of 26 dB.

D. Experimental Result Analysis

The experimental results are presented in Table. XI and from Fig. 10 to Fig. 15. Table. XI contains all SNDR measures and classical linearity metrics measures. The results from Fig. 10 to Fig. 12 refer to swept-tone NPR measures done with the
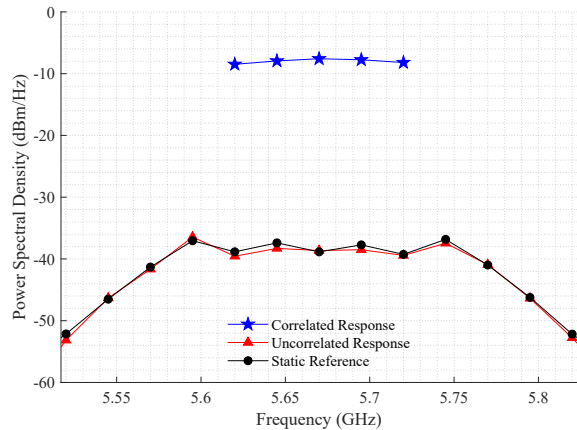

Fig. 10. Era-2+ - 5-tone excitation - correlated response and uncorrelated IMD profiles (Measurement and Reference).
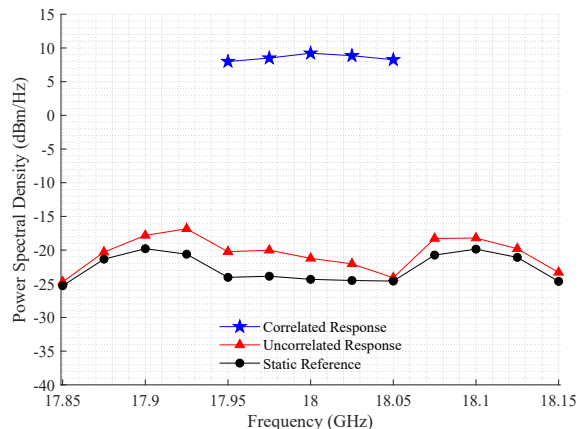

Fig. 11. ZVA-213-S+ - 5-tone excitation - correlated response and uncorrelated IMD profiles (Measurement and Reference).
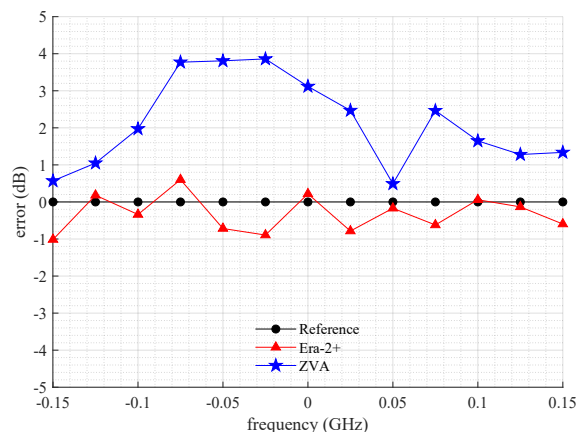

Fig. 12. 5-tone excitation - error between uncorrelated response and reference profile (Era-2+ and ZVA-213-S+). The error curves, even though referent to different carrier frequencies, are plotted in the same graph to facilitate the comparison between the two dynamic behaviors.
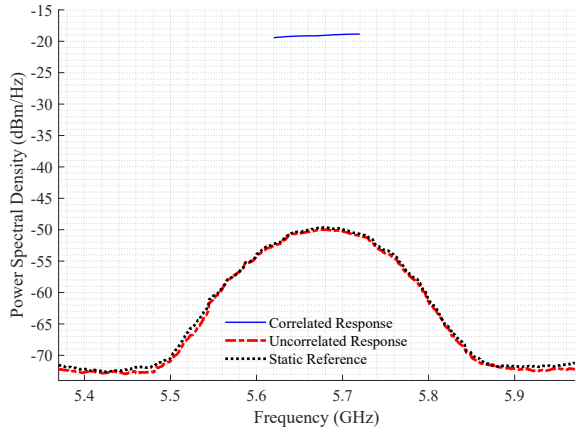
Fig. 13. Era-2+ - 101-tone excitation - correlated response and uncorrelated IMD profiles (Measurement and Reference).
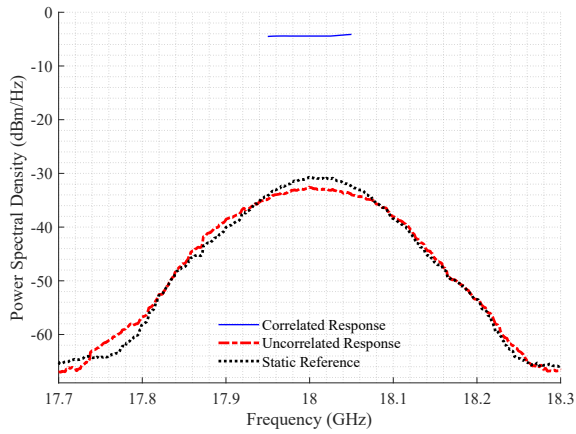

Fig. 14. ZVA-213-S+ - 101-tone excitation - correlated response and uncorrelated IMD profiles (Measurement and Reference).
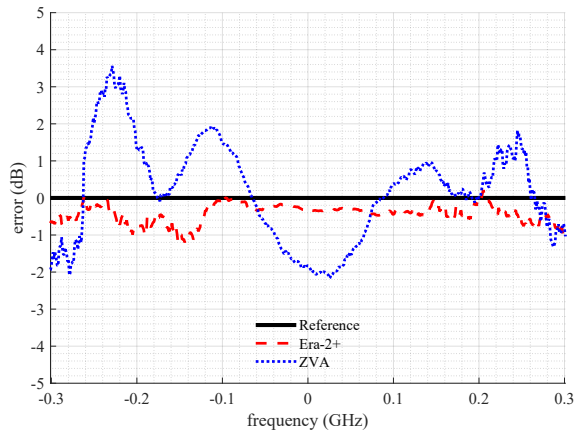

Fig. 15. 101-tone excitation - error between uncorrelated response and reference profile (Era-2+ and ZVA-213-S+). The error curves, even though referent to different carrier frequencies, are plotted in the same graph to facilitate the comparison between the two dynamic behaviors.

TABLE XI
EXPERIMENTAL RESULTS: IMD POWER METRICS AND SNDR

Metric	$ACPR_L$	$ACPR_U$	NPR	CCPR	**SNDR**
Unit	dB	dB	dB	dB	**dB**
Era_m (5-tones)	33.9	34.4	30.7	30.8	**28.0**
Era_r (5-tones)	34.2	33.9	30.8	30.3	**27.6**
Zva_m (5-tones)	28.6	29.0	29.8	29.9	**24.3**
Zva_r (5-tones)	30.6	30.5	32.6	32.6	**26.2**
Era_m (101-tones)	52.4	47.3	26.9	30.2	**28.8**
Era_r (101-tones)	50.9	46.5	27.1	29.9	**28.5**
Zva_m (101-tones)	47.1	41.8	22.9	27.8	**25.8**
Zva_r (101-tones)	48.3	41.3	21.7	26.1	**24.8**

5-tone excitation, whereas the results from Fig. 13 to Fig. 15 refer to swept-tone NPR measures done with the 101-tone excitation. For each measurement performed, each metric was also evaluated taking into account the reference profile, instead of the measured uncorrelated IMD profile. These results are also listed in Table. XI to aid the result analysis.

Lets start with the Era-2+ characterization performed with 5-tones. As shown in Fig. 10, the uncorrelated IMD profile and the reference profile overlap. Fig. 12 confirms this assessment, showing that for this device the error between uncorrelated IMD profile and reference is mostly constant throughout the band, and that the magnitude of the error never exceeds 1 dB. Beyond this, the error between uncorrelated IMD profile and the reference profile for all the metrics listed in Table. XI never exceeds 0.5 dB. All these results evidence a memoryless behavior, as expected. The swept-tone NPR measure provides more frequency resolution than the metrics listed in Table. XI, which for this memoryless scenario does not provide any additional information.

The advantages of the swept-tone NPR measures are clear in the 5-tone experimental results of the ZVA-213-S+ device. As shown in Fig. 11, the uncorrelated IMD profile is above the reference throughout the band. The most noticeable feature of these profiles is the decreasing error between the uncorrelated IMD profile and the reference along the co-channel frequencies. For this device, the error curve, shown in Fig. 12, reveals more details. It can be noted that lower-band adjacent-channel error increases towards the co-channel, whereas higher-band adjacent-channel error is mostly constant, around 1.5 dB. The frequency dependence of the error between uncorrelated IMD profile and reference confirms the presence of nonlinear dynamics in the IMD response of the ZVA-213-S+ device. Regarding $ACPR_L$ and $ACPR_U$ metrics, a 1.5 dB error is measured between the uncorrelated IMD profile and the reference profile evaluations, as listed in Table. XI. These metrics can detect that the uncorrelated IMD profile is above the reference, but loose the information regarding the adjacent-channel error trend. Similar considerations can be made about the NPR and CCPR metrics. Errors of 2.8 dB can detect that the uncorrelated IMD profile is above the reference, but the perception that the error decreases along the co-channel is lost. In the presence of nonlinear dynamics, it is clear that swept-tone NPR measurements can provide detailed information that

classic metrics neglect.

Now, consider the Era-2+ characterization performed with 101-tones. Once again, the uncorrelated IMD profile and the reference overlap, as show in Fig. 13. For this excitation the error between the uncorrelated IMD profile and the reference remains constant throughout the band, and lower than 1 dB in modulus, as depicted in Fig. 15. Apart from the adjacent-channel measures, all metrics agree with the reference metric with an error lower than 0.3 dB, as listed in Table. XI. The adjacent channel error is slightly larger - 1.5 dB - because these measures are taken at lower powers, where small absolute errors translate into larger relative errors. Despite this limitation in the evaluation of ACPR, the experimental results, particularly the error curves in Fig. 15, confirm the memoryless behaviour of the Era-2+, now under a 101-tone excitation.

Finally, lets analyze the ZVA-213-S+ characterization performed with 101-tones. Once again, the uncorrelated IMD profile and the reference do not overlap, as shown in Fig. 14. But the uncorrelated IMD trend is now more complex than observed for the 5-tone excitation. There are several frequency bands in which the uncorrelated IMD profile is either above, bellow, or overlapped with the reference, as can be clearly observed in Fig. 15. Once again, the frequency dependence of the error between uncorrelated IMD profile and reference confirms the presence of nonlinear dynamics in the IMD response of the ZVA-213-S+ device. It is interesting to contrast the error profile, depicted in Fig. 15, with classical linearity measures, listed in Table. XI. The ACPR_L measure is 1.2 dB bellow the reference ACPR_L. Looking into the error curve it is perceptible that this skew occurs because in the lower-band adjacent-channel the cumulative uncorrelated IMD power above the reference is higher than the cumulative uncorrelated IMD power bellow the reference. In the higher-band adjacent channel the impacts of the cumulative analysis are more severe, because the amount of comulative uncorrelated IMD power above and bellow the reference is similar. Therefore, the error between the uncorrelated IMD profile and the reference in the ACPR_U measure is only 0.5 dB, which can mask the detection of nonlinear dynamics. Note, again, how the cumulative nature of classic linearity metrics mask important features of IMD profiles containing nonlinear dynamic effects. Regarding the NPR and CCPR, errors of 1.2 dB and 1.7 dB are measured in relation to the reference, respectively. These errors detect that the uncorrelated IMD profile is bellow the reference in the co-channel, but the perception of the error trend is lost.

It is now important to compare the experimental results obtained for the 5-tone excitation with the results obtained for the 101-tone excitation. For the Era-2+, the uncorrelated IMD responses and the error trends reinforce each other, confirming the memoryless behavior of the device. The same can be said for the ZVA-213-S+ device, in the sense that nonlinear dynamic effects are detected with both signals. However, more work is required to establish an identity between these two regimes of operation in order to be able to perform a direct comparison between the results obtained from each excitation, because IMD profiles and error trends are dependent on input excitation, as previously explained. The ACPR and NPR measures vary significantly from one excitation to the other, which makes them difficult to compare. The CCPR measure is similar for the memoryless scenario, but in the presence of memory effects errors can be as large as 6.5 dB. However, the SNDR measures, evaluated as defined in (23), agree within a 1.5 dB error margin.

Regarding linearity metrics, in a memoryless scenario all metrics evaluated provide IMD measures with similar levels of confidence. In the presence of nonlinear dynamics, the error profile obtained from swept-tone NPR is the most informative metric. The remaining metrics can be misleading, as demonstrated by the experiments. In sum, swept-tone NPR is capable of reliably distinguishing nonlinear dynamic scenarios from memoryless scenarios, while accurately evaluating IMD power levels.

Regarding the device under test performance evaluation, the Era-2+ device is a static nonlinear device that exhibits a 28.8 dB SNDR at 1 dBm of output power when excited at 5.67 GHz, whereas the ZVA-213-S+ device is a nonlinear dynamic device that exhibits a 25.8 dB SNDR at 15.6 dBm of output power when excited at 18 GHz. In these conditions the Era-2+ SNDR is 3 dB higher than the ZVA-213-S+, meaning that a higher portion of the output power is desired signal power. In that sense, it can be said that Era-2+ device is more linear at delivering 1 dBm of output power at a 5.67 GHz carrier, than the ZVA-213-S+ device at delivering 15.6 dBm of output power at an 18 GHz carrier. This analysis is not an absolute comparison of the performance of the devices, because the regimes of operation are too distinct, it is just to provide an idea of how to use the proposed metrics to evaluate both dynamics and linearity.

As a final note, observe that it was the definition of the static reference that allowed an objective interpretation of the experimental results for every linearity metric considered.

VIII. CONCLUSION

This work presented a theoretical framework capable of analyzing IMD profiles produced under multi-tone excitation and detecting the impacts of nonlinear dynamic effects. This analysis exposed critical limitations of classic linearity metrics in the assessment of IMD responses produced by nonlinear dynamic RF systems, and allowed for the definition of general characterization guidelines to overcome those limitations.

Based on these contributions, a novel characterization method, based on classic NPR procedures, for the characterization of IMD profiles affected by nonlinear dynamic effects was proposed and validated experimentally.

The proposed method, swept-tone NPR, contemplates several advantages over previous works addressing NPR characterization, as the novel method:

1) does not require an AWGN excitation. It is consistent for different multi-tone excitation statistics, and can be adapted to excitations used in practical scenarios;
2) it captures full inband IMD (adjacent-channel + co-channel IMD)

3) it separates the correlated inband response, from the uncorrelated inband response. This allows for an accurate evaluation of inband SNDR;

4) it is capable of distinguishing memoryless scenarios from nonlinear dynamic scenarios;

5) it defines a frequency dependent metric, which allows for the detection fine IMD profile features introduced by nonlinear dynamic effects, both in adjacent channel and co-channel frequencies;

6) it is not bound to specific nonlinear mechanisms.

The general characterization guidelines presented are good practices that allow for the definition of novel characterization methods, or for the adaptation of exiting methods, to reliably capture IMD profiles affected by nonlinear dynamic effects in accordance to specific RF application constraints. This is particularly important, as RF applications continue to expand towards broader instantaneous bandwidths and nonlinear dynamic effects become more relevant.

Further work is required to establish direct relationships between experimental results obtained with different excitation signals, but the initial results presented here indicate the ability to correctly characterize IMD power level while detecting nonlinear dynamic effects.

The developments presented in this work can be used in design, modeling and compensation of nonlinear dynamic RF systems. However, future developments are required in this regard, so that reliable linearity metrics, contemplating nonlinear dynamic effects in broadband scenarios, are integrated in these fields, finally replacing simpler, but invalid, metrics in these domains of application.

REFERENCES

[1] C. Boulanger, A. Mallet, J. Puech, L. Lapierre, and J. Sombrin, "A new criterion for power amplifier comparison and optimisation," in *IEE Seminar on Microwave and RF Power Amplifiers (Ref. No. 2000/118)*, 2000, pp. 1/1–1/6.

[2] A. Mallet, F. Gizard, T. Reveyrand, L. Lapierre, and J. Sombrin, "A new satellite repeater amplifier characterization system for large bandwidth NPR and modulated signals measurements," in *2002 IEEE MTT-S International Microwave Symposium Digest (Cat. No.02CH37278)*, vol. 3, 2002, pp. 2245–2248 vol.3.

[3] P. Medrel, T. Reveyrand, A. Martin, P. Bouysse, J.-M. Nébus, and J. Sombrin, "Time domain envelope characterization of power amplifiers for linear and high efficiency design solutions," in *WAMICON 2013*, 2013, pp. 1–6.

[4] K. M. Gharaibeh, K. G. Gard, and M. B. Steer, "Accurate estimation of digital communication system metrics-SNR, EVM and /spl rho/ in a nonlinear amplifier environment," in *64th ARFTG Microwave Measurements Conference, Fall 2004.*, 2004, pp. 41–44.

[5] J. B. Sombrin, "On the formal identity of EVM and NPR measurement methods: conditions for identity of error vector magnitude and noise power ratio," in *2011 41st European Microwave Conference*, 2011, pp. 337–340.

[6] Y. Rolain, M. Zyari, E. Van Nechel, and G. Vandersteen, "A measurement-based error-vector-magnitude model to assess non linearity at the system level," in *2017 IEEE MTT-S International Microwave Symposium (IMS)*, 2017, pp. 1429–1432.

[7] E. Van Nechel, Y. Rolain, and J. Lataire, "Extracting improved figures of merit for characterizing nonlinear devices using multisine excitation signals," in *2018 91st ARFTG Microwave Measurement Conference (ARFTG)*, 2018, pp. 1–4.

[8] J. Lajoinie, E. Ngoya, D. Barataud, J. Nebus, J. Sombrin, and B. Rivierre, "Efficient simulation of NPR for the optimum design of satellite transponders SSPAs," in *1998 IEEE MTT-S International Microwave Symposium Digest (Cat. No.98CH36192)*, vol. 2, 1998, pp. 741–744 vol.2.

[9] T. Reveyrand, D. Barataud, J. Lajoinie, M. Campovecchio, J.-M. Nebus, E. Ngoya, J. Sombrin, and D. Roques, "A novel experimental noise power ratio characterization method for multicarrier microwave power amplifiers," in *55th ARFTG Conference Digest*, vol. 37, 2000, pp. 1–5.

[10] S. Din, A. M. Morishita, N. Yamamoto, C. Brown, M. Wojtowicz, and M. Siddiqui, "High-power K-band GaN PA MMICs and module for NPR and PAE," in *2017 IEEE MTT-S International Microwave Symposium (IMS)*, 2017, pp. 1838–1841.

[11] G. Lasser, M. R. Duffy, and Z. Popović, "Dynamic dual-gate bias modulation for linearization of a high-efficiency multistage PA," *IEEE Trans. Microw. Theory Techn.*, vol. 67, no. 7, pp. 2483–2494, 2019.

[12] S. Laurent, J. P. Teyssier, R. Quere, J. Sombrin, and M. Prigent, "Linearity characterization of RF circuits through an unequally spaced multi-tone signal," in *2016 88th ARFTG Microwave Measurement Conference (ARFTG)*, 2016, pp. 1–4.

[13] V. Gillet, M. Bouslama, J. Teyssier, M. Prigent, J. Nallatamby, and R. Quéré, "An unequally spaced multi-tone load–pull characterization technique for simultaneous linearity and efficiency assessment of RF power devices," *IEEE Trans. Microw. Theory Techn.*, vol. 67, no. 7, pp. 2505–2513, 2019.

[14] V. Gillet, J. P. Teyssier, A. Al Hajjar, A. Gasmi, C. E. Kacou, M. Prigent, and R. Quéré, "Millimeter-wave power amplifier linearity characterization using unequally spaced multi-tone stimulus," in *2020 IEEE/MTT-S International Microwave Symposium (IMS)*, 2020, pp. 755–758.

[15] J. Teyssier, J. Dunsmore, J. Verspecht, and J. Kerr, "Coherent multi-tone stimulus-response measurements with a VNA," in *2017 89th ARFTG Microwave Measurement Conference (ARFTG)*, 2017, pp. 1–3.

[16] A. Geens, Y. Rolain, W. Van Moer, K. Vanhoenacker, and J. Schoukens, "Discussion on fundamental issues of NPR measurements," *IEEE Trans. Instrum. Meas.*, vol. 52, no. 1, pp. 197–202, 2003.

[17] J. C. Pedro and N. B. Carvalho, *Intermodulation distortion in microwave and wireless circuits*. Artech House, 2003.

[18] N. B. De Carvalho and J. C. Pedro, "A comprehensive explanation of distortion sideband asymmetries," *IEEE Trans. Microw. Theory Techn.*, vol. 50, no. 9, pp. 2090–2101, 2002.

[19] J. P. Martins, N. B. Carvalho, and J. C. Pedro, "Intermodulation distortion of third-order nonlinear systems with memory under multisine excitations," *IEEE Trans. Microw. Theory Techn.*, vol. 55, no. 6, pp. 1264–1271, 2007.

[20] S. Farsi, P. Draxler, H. Gheidi, B. K. Nauwelaers, P. Asbeck, and D. Schreurs, "Characterization of intermodulation and memory effects using offset multisine excitation," *IEEE Trans. Microw. Theory Techn.*, vol. 62, no. 3, pp. 645–657, 2014.

[21] R. Figueiredo, A. Piacibello, V. Camarchia, and N. B. Carvalho, "Swept notch NPR for linearity assessment of systems presenting long-term memory effects," in *2020 95th ARFTG Microwave Measurement Conference (ARFTG)*, 2020, pp. 1–4.

[22] J. C. Pedro and N. B. de Carvalho, "Characterizing nonlinear RF circuits for their in-band signal distortion," *IEEE Trans. Instrum. Meas.*, vol. 51, no. 3, pp. 420–426, 2002.

[23] J. C. Pedro and N. B. De Carvalho, "On the use of multitone techniques for assessing RF components' intermodulation distortion," *IEEE Trans. Microw. Theory Techn.*, vol. 47, no. 12, pp. 2393–2402, 1999.

[24] A. Walker, M. Steer, K. Gard, and K. Gharaibeh, "Multi-slice behavioral model of RF systems and devices," in *Proceedings. 2004 IEEE Radio and Wireless Conference (IEEE Cat. No. 04TH8746)*, 2004, pp. 71–74.

[25] J. P. Martins, P. M. Cabral, N. Borges Carvalho, and J. C. Pedro, "A metric for the quantification of memory effects in power amplifiers," *IEEE Trans. Microw. Theory Techn.*, vol. 54, no. 12, pp. 4432–4439, 2006.

[26] N. B. Carvalho and D. Schreurs, *Microwave and wireless measurement techniques*. Cambridge University Press, 2013.

[27] N. B. Carvalho, K. A. Remley, D. Schreurs, and K. G. Gard, "Multisine signals for wireless system test and design [application notes]," *IEEE Microw. Mag.*, vol. 9, no. 3, pp. 122–138, 2008.

[28] Mini-Circuits. (2020) Drop-in monolithic amplifier. [Online]. Available: https://www.minicircuits.com/pdfs/ERA-2+.pdf

[29] ——. (2020) Super ultra wideband amplifier. [Online]. Available: https://www.minicircuits.com/pdfs/ZVA-213-S+.pdf

Ricardo Figueiredo (Graduate Student Member, IEEE) was born in Viseu, Portugal, in 1995. He received the M.Sc. degree in electronics and telecomumunications engineering from the Universidade de Aveiro, Aveiro, Portugal, in 2018, where he is currently pursuing the Ph.D. degree in electrical engineering.

He is currently a Researcher at the Instituto de Telecomumicações, Aveiro. His main research interests include nonlinear instrumentation and nonlinear characterization of microwave systems.

Mr. Figueiredo a is member of the IEEE MTT-S Student Branch Chapter at Universidade de Aveiro.

Nuno Carvalho (Fellow, IEEE) was born in Luanda, Angola, in 1972. He received the Diploma and Doctoral degrees in electronics and telecommunications engineering from the University of Aveiro, Aveiro, Portugal, in 1995 and 2000, respectively.

He is currently a Full Professor and a Senior Research Scientist with the Institute of Telecommunications, University of Aveiro and an IEEE Fellow. He coauthored Intermodulation in Microwave and Wireless Circuits (Artech House, 2003), Microwave and Wireless Measurement Techniques (Cambridge University Press, 2013), White Space Communication Technologies (Cambridge University Press, 2014) and Wireless Power Transmission for Sustainable Electronics (Wiley, 2020). He has been a reviewer and author of over 200 papers in magazines and conferences. He is the Editor in Chief of the Cambridge Wireless Power Transfer Journal, an associate editor of the IEEE Microwave Magazine and former associate editor of the IEEE Transactions on Microwave Theory and Techniques and IET Microwaves Antennas and Propagation Journal. He is the co-inventor of six patents. His main research interests include software-defined radio front-ends, wireless power transmission, nonlinear distortion analysis in microwave/wireless circuits and systems, and measurement of nonlinear phenomena. He has recently been involved in the design of dedicated radios and systems for newly emerging wireless technologies.

Dr. Borges Carvalho is a member of the IEEE MTT ADCOM, the past-chair of the IEEE Portuguese Section, MTT-20 and MTT-11 and also belong to the technical committees, MTT-24 and MTT-26. He is also the vice-chair of the URSI Commission A (Metrology Group). He was the recipient of the 1995 University of Aveiro and the Portuguese Engineering Association Prize for the best 1995 student at the University of Aveiro, the 1998 Student Paper Competition (Third Place) of the IEEE Microwave Theory and Techniques Society (IEEE MTT-S) International Microwave Symposium (IMS), and the 2000 IEE Measurement Prize. He is a Distinguished Lecturer for the RFID-Council and was a Distinguished Microwave Lecturer for the IEEE Microwave Theory and Techniques Society.

Anna Piacibello (Member, IEEE) was born in Chivasso, Italy, in 1991. She received the Bachelor and Master degrees in Electronic Engineering from the Politecnico di Torino in 2013 and 2015, respectively.

In 2017, she was a visiting researcher at the Centre for High Frequency Engineering (CHFE) of Cardiff University. She received the PhD degree cum laude in Electric, Electronic and Communication Engineering from the Politecnico di Torino in 2019. Her current research interests include broadband and highly efficient microwave power amplifiers. Dr. Piacibello is currently a postdoctoral research associate with the Department of Electronics and Telecommunications, Politecnico di Torino, Italy, and with the Microwave Engineering Center for Space Applications, Rome, Italy.

She was a recipient of the 2018 Young Engineer Prize awarded by the EuMA association.

Vittorio Camarchia (Senior Member, IEEE) was born in Turin, Italy, in 1972. He received the Laurea degree and Ph.D. degree in Electronic Engineering from the Politecnico di Torino, Turin, Italy, in 2000 and 2003, respectively.

He was in 2001-2003 a Visiting Researcher with the Electrical and Computer Engineering Department, Boston University. Since 2004 he joined the Department of Electronics and Telecommunications of the Politecnico di Torino where he is presently an Associate Professor. His research is focused on modeling, design and characterization of RF and microwave modules and systems. He is the p.i. of projects for the European Space Agency (ESA), reviewer of the Research Executive Agency of the European Commission for space-related topics and of the major journal of the field. He has published 180 peer-reviewed papers, two books and several book chapters.

Prof. Camarchia is member of the IEEE MTT-S Subcommittees 12 on power amplifiers and 23 on Wireless Communications and serves as member of the International Microwave Symposium Technical Program Review Committee on power amplifiers. He is associate editor of the IEEE Transactions on Microwave Theory and Techniques and of IEEE Access, and has been the Guest editor of the 2020 Special Issue on Broadband Millimeter-wave Power Amplifiers of the IEEE Transactions on Microwave Theory and Techniques. He was a recipient of the 2002 Young Graduated Research Fellowship presented by the GAAS Association.